Available online at www.sciencedirect.com
ScienceDirect
Trans. Nonferrous Met. Soc. China 32(2022) 604−617
Transactions of Nonferrous Metals Society of China
www.tnmsc.cn

Hydrogen storage properties of magnesium hydride catalyzed by Ni-based solid solutions

Jian ZHANG[1,2], Liu HE [1], Yuan YAO[1], Xiao-jie ZHOU[1], Li-kun JIANG[1], Ping PENG[3]

1. Hunan Provincial Key Laboratory of Intelligent Manufacturing Technology for High-performance Mechanical Equipment, Changsha University of Science and Technology, Changsha 410114, China;
2. Hunan Provincial Key Laboratory of Materials Protection for Electric Power and Transportation, Changsha University of Science and Technology, Changsha 410114, China;
3. College of Materials Science and Engineering, Hunan University, Changsha 410082, China

Received 14 March 2021; accepted 10 September 2021

Abstract: The Ni−25%X (X=Fe, Co, Cu, molar fraction) solid solutions were prepared and then doped into MgH_2 through high-energy ball milling. The initial dehydrogenation temperatures of MgH_2/Ni−25%X composites are all decreased by about 90 °C relative to the as-milled pristine MgH_2. The Ni−25%Co solid solution exhibits the most excellent catalytic effect, and the milled MgH_2/Ni−25%Co composite can release 5.19 wt.% hydrogen within 10 min at 300 °C, while the as-milled pristine MgH_2 can only release 1.78 wt.% hydrogen. More importantly, the dehydrogenated MgH_2/Ni−25%Co composite can absorb 5.39 wt.% hydrogen at 275 °C within 3 min. The superior hydrogen sorption kinetics of MgH_2/Ni−25%Co can be ascribed to the actual catalytic effect of in-situ formed Mg_2Ni(Co) compounds. First-principles calculations show that the hydrogen absorption/desorption energy barriers of Mg/MgH_2 systems decrease significantly after doping with transition metal atoms, which interprets well the improved hydrogen sorption properties of MgH_2 catalyzed by Ni-based solid solutions.

Key words: MgH_2; Ni-based solid solutions; catalytic effect; hydrogen storage properties; first-principles calculations

1 Introduction

The traditional fossil fuels, such as coal, oil, and natural gas, have become a powerful driving force for the development of the world economy since the second industrial revolution. Especially from the beginning of the 21st century, the trade activities between countries become increasingly frequent with the development of economic globalization, making the demand for energy in human society continue to expand. However, the current use of energy by countries around the world is still at the level of traditional fossil energy [1]. Their massive use has brought many environment problems, such as global warming, air pollution, and water pollution [2]. In order to realize the sustainable development of human society, it is urgent to seek a cheap, clean, and renewable energy source. In the past few decades, the researchers have conducted many explorations on replacing traditional fossil fuels with clean and renewable energy sources, such as wind energy, tidal energy, geothermal energy, solar energy, nuclear energy and hydrogen energy [3]. Among them, hydrogen energy is considered to be the most ideal clean energy in the future due to its wide range of sources, high energy density, clean and non-toxic combustion products [4−7].

Although hydrogen energy exhibits the broad development prospects, providing safe and efficient hydrogen storage methods is still the key bottleneck

Corresponding author: Jian ZHANG, Tel: +86-731-85258644, E-mail: zj4343@163.com; Xiao-jie ZHOU, E-mail: xjzhoucsu@163.com
DOI: 10.1016/S1003-6326(22)65819-9

for the realization of hydrogen economy. The currently used hydrogen storage methods are mainly composed of gaseous, liquid and solid-state hydrogen storage [8−12]. Among solid-state hydrogen storage methods, metal hydrides are widely favored by researchers owing to their safety and high efficiency. A large number of studies have shown that magnesium hydride (MgH_2) is a potential solid-state hydrogen storage material among numerous metal hydrides due to its high reversible hydrogen mass capacity (7.6 wt.%), high volume capacity (110 g/L), abundant raw material sources and low cost [13,14].

Despite many advantages of MgH_2, its high thermodynamic stability, slow hydrogen sorption kinetics and poor cycle performance make its wide application face huge challenges [15,16]. In the past few decades, the researchers have performed numerous modification studies to improve the hydrogen storage properties of MgH_2. So far, the modification strategies can be mainly divided into catalyzing [17−28], nanosizing [29−34] and alloying [35−40], etc., among which catalyzing is one of the most effective modification means. A variety of catalysts, such as transition-metal (e.g., Ti, V, Nb, Fe, Co, Ni, Cu, Zn) and their compounds (e.g., hydrides, carbides, nitrides, oxides, fluorides, halides), intermetallics, and some nonmetallic materials (e.g., graphite, graphene, carbon nanotubes) have been reported to play significant roles in enhancing the hydrogen storage properties of MgH_2 [17]. In particular, the Ni-based catalysts show superior catalytic effect on the dehydrogenation/hydrogenation kinetics of MgH_2. For example, XIE et al [41] systematically investigated the effects of Ni on the dehydrogenation performance of MgH_2. They found that Ni facilitated the nucleation of magnesium phase and accelerated the recombination of hydrogen atoms during the dehydrogenation of MgH_2, and the activation energy decreases with increasing nickel content. Based on the excellent catalytic effect of metal Ni, the researchers further studied the synergistic catalytic effect of Ni and carbon materials on MgH_2. For example, MENG et al [17] reported an electrospinning-based reduction approach to in situ generate nanostructured nickel catalyst in carbon nanofibers (Ni@C). They found that the prepared Ni@C showed a remarkable catalytic effect on improving the hydrogen storage properties of MgH_2. Compared with the as-milled MgH_2, the dehydrogenation capacity of the MgH_2−10wt.%Ni@C composite was observably increased. Simultaneously, the dehydrogenation activation energy of MgH_2−10wt.%Ni@C was 93.08 kJ/mol, which was 94.33 kJ/mol lower than that of the as-milled MgH_2. YAO et al [20] prepared uniformly dispersed Ni nanoparticles (NPs) anchored on reduced graphene oxide (Ni@rGO) to catalyze the dehydrogenation/hydrogenation of MgH_2. The onset dehydrogenation temperature of MgH_2 decreased from 251 to 190 °C. Meanwhile, HUANG et al [42] found that the MgH_2+ 10wt.%Ni@C-MXene also exhibited high cycling stability and eminent hydrogen sorption kinetics.

The researchers further explored the role of Ni-based catalysts in improving the hydrogen storage properties of MgH_2 based on the excellent catalytic effect of metal Ni and carbon materials. For example, CHENG et al [43] synthesized bimetallic Pd−Ni nanoparticles supported by mesoporous carbon material CMK-3 ($Pd_{30}Ni_{70}$/CMK-3) through hydrogen reduction methods and solution impregnation. They found that the initial dehydrogenation temperature of MgH_2-$Pd_{30}Ni_{70}$/CMK-3 decreased from 593 K of pristine MgH_2 to 435 K, and the hydrogen storage properties of MgH_2 at low temperatures were improved significantly. They attributed the enhanced hydrogen storage properties of MgH_2 to the synergistic effects of destabilization and catalysis of nano-dispersed Pd and Ni particles. In addition, the original core-shell CoNi@C bimetallic nanoparticles were also used to improve the dehydrogenation/hydrogenation kinetics of MgH_2. ZHAO et al [44] showed that the dehydrogenation of the MgH_2−8wt.%CoNi@C started at 173 °C, and the dehydrogenation capacity was 5.83 wt.% within 1800 s at 275 °C. More importantly, the system could absorb 4.83 wt.% hydrogen even at 1800 s and a low temperature of 100 °C. They suggested that the reversible phase transitions of Mg_2Co/Mg_2CoH_5 and Mg_2Ni/Mg_2NiH_4, and the confinement effect of carbon shell were the key factors for the obvious improvement of hydrogen storage properties of MgH_2. In our recent work [45], the modification effects of NiCu solid solutions with different molar ratios on improving hydrogen storage properties of MgH_2 were systematically investigated. It was found that the MgH_2/

Ni−50%Cu system could not only release 5.14 wt.% hydrogen within 15 min at 300 °C, but also absorb 4.37 wt.% hydrogen at 250 °C within 30 min. The enhanced hydrogen sorption kinetics of MgH_2/Ni−50%Cu mainly attributes to the "hydrogen spillover" effect of in-situ formed Mg_2Ni(Cu) phases.

In view of the excellent catalysis of Ni-based solid solution, we further studied and compared the effects of NiCo, NiCu and NiFe solid solutions on the hydrogen storage properties of MgH_2 in this work. According to the knowledge of phase diagram, Cu and Fe can realize infinite solid solution in Ni, while the maximum molar fraction of Co in Ni solid solution is 25%. Thus, the Ni−25%Co, Ni−25%Cu and Ni−25%Fe solid solutions were prepared by high-energy ball milling in this work. Then, the catalytic effects of these solid solutions on the hydrogen absorption/desorption properties of MgH_2 were investigated and compared. Furthermore, first-principles calculations were performed to explain the corresponding catalysis mechanisms of Ni-based solid solutions. The obtained results will enrich the Ni-based solid solution catalysts system and provide an important guidance for designing more transition metal solid solutions to improve the hydrogen storage properties of magnesium-based and other metal-based hydrides.

2 Experimental

2.1 Samples preparation

In this work, the Fe powder (99.5 wt.%), Co powder (99.8 wt.%), Ni powder (99.8 wt.%) and Cu powder (99.9 wt.%) were obtained from Alfa Aesar. The MgH_2 powder (98 wt.%) was commercially got from Saiamin Chemical Co., Ltd. All as-received powders were directly used without further purification. Firstly, the Ni−25%X (X=Fe, Co, Cu) solid solutions were prepared by high-energy ball milling (Ni/X molar ratio was 3:1). For comparison, the pristine Ni was also milled under the same condition. Then, the obtained Ni−25%X (X=Fe, Co, Cu) solid solutions and Ni powder after ball milling were further mixed with MgH_2 with a mass ratio of 1:9. At the same time, the as-milled pristine MgH_2 was used to compare with these catalysts-doped systems under the same ball milling conditions. The mill used was a QM−3C high-speed vibration ball mill with a stainless-steel tank. The balls of 10 mm in diameter made of stainless steel (SUS304) were employed. All samples were ball milled at 1000 r/min of rotational speed for 5 h with the ball to powder mass ratio of 30:1. In order to avoid the excessively temperature elevation during the ball milling, these samples were stopped to cool for 10 min at every 1 h. All operations on the samples were carried out under high purity argon (99.999 vol.%) atmosphere in a glove box with water/oxygen concentrations lower than 0.1 r/min.

2.2 Samples characterization

The phase structures of samples were characterized by using X-ray diffraction (XRD) apparatus (Rigaku D/Max 2500) with Cu K_α radiation at a scanning rate of 0.02 (°)/0.15 s, in the 2θ range between 5° and 90°. Diffraction data were recorded at room temperature, and the current and voltage were 250 mA and 40 kV, respectively. The Rietveld refinement method based on XRD patterns was used to calculate and refine the lattice parameters of different phases. Scanning electron microscopy (SEM) (TESCAN MIRA 3LMU/X-Max20/H1002) equipped with energy dispersive spectrometer (EDS) microanalysis and a backscattered mode, and transmission electron microscopy (TEM) (JEM2100F) were employed to characterize the microstructures of samples. The non-isothermal dehydrogenation performance (temperature programmed desorption (TPD)) and isothermal hydrogen adsorption/desorption kinetics of samples were tested using a Sieverts type volumetric apparatus (University of Science and Technology Beijing, and Yongxing Technology Co., Ltd). The samples were heated from room temperature to 500 °C at a heating rate of 3 °C/min during TPD test. The isothermal hydrogen absorption/desorption kinetics curves of samples were obtained at different temperatures (i.e., 250, 275 and 300 °C, respectively). The initial hydrogen pressures of MgH_2/Ni−25%X (X=Fe, Co, Cu) systems for hydrogen desorption and absorption are 0.003 and 3.0 MPa, respectively.

2.3 Computational methods

All calculations were carried out by using first-principles plane-wave pseudopotential method as implemented in Cambridge Sequential Total Energy Package (CASTEP) code based on density

functional theory (DFT) [46]. The Generalized Gradient Approximation (GGA) of Perdew-Burke-Ernzerhof (PBE) functional [47] was adopted to describe the exchange-correlation energy and the plane wave cutoff energy with 400 eV was employed in this work. The convergences criteria of the variable-cell relaxation and transition state (TS) search were 1.0×10^{-5} eV/atom, 0.03 eV/Å, 0.05 GPa and 0.001 Å for energy, force, stress and displacement, respectively.

3 Results and discussion

3.1 Structural and morphological characterizations of Ni−25%X solid solutions and MgH_2/Ni−25%X composites

Figure 1 shows the XRD patterns of pristine Ni powder and Ni−25%X (X=Fe, Co, Cu) after ball milling for 5 h. All the samples are composed of three diffraction peaks corresponding to (111), (200) and (220) planes, respectively, as shown in Fig. 1(a). For pristine Ni, the three characteristic peaks are distributed at 44.5°, 51.8° and 76.3°, respectively. After Fe, Co and Cu doping, the diffraction peaks of samples all shift to the left and no new phase is detected, as shown in Fig. 1(b). Furthermore, the lattice parameters of the as-milled Ni−25%X samples are refined by the Rietveld refinement method, and the obtained results exclude that the left deviation of diffraction peaks is caused by sampling shift or zero shift during scanning. This indicates that the Ni−25%X solid solutions are successfully synthesized through ball milling. The lattice expansion of Ni after X (X=Fe, Co, Cu) doping should be ascribed to the larger atomic radius of X (Fe=1.26 Å, Co=1.25 Å, Cu=1.28 Å) atom relative to Ni (1.24 Å), which results in the left shift of the diffraction peaks for the Ni−25%X solid solutions.

Figure 2 presents the SEM images of Ni−25%X solid solutions with different magnifications. It can be seen that the particle size of these solid solutions is decreased in the order of Ni−25%Cu, Ni−25%Co, and Ni−25%Fe. For Ni−25%Fe system, its particle distribution is relatively uniform, and the size varies from 1 to 5 μm, as shown in Figs. 2(a) and (d). Compared with Ni−25%Fe system, the particle size of Ni−25%Co is significantly larger, which is mainly concentrated in 3−5 μm, as shown in Figs. 2(b) and (e). For Ni−25%Cu system, the particles are relatively coarse, and their sizes are larger than 5 μm, as shown in Figs. 2(c) and (f). As we all know, the elastic constants determine the response of crystal to external force, and they play an important role in the mechanical properties of material. In order to explain the relationship between the morphologies and mechanical properties of Ni−25%X solid solutions, the elastic properties of Ni crystal doped with 25 at.% X (X=Fe, Co, Cu) atom are calculated by a stress−strain approach. The ductility/brittleness of a crystal is usually judged by the quotient of its shear modulus G to bulk modulus B, i.e., G/B [48]. According to the Pugh criterion [49], the G/B value of 0.57 is the critical value for judging the ductility/brittleness of crystal. Generally, a crystal is regarded as ductile if G/B value is less than 0.57, and vice versa. The calculated G/B values of Ni−25%Fe, Ni−25%Co and Ni−25%Cu solid solutions in this work are 0.46, 0.45, and 0.41 respectively, which are all lower than 0.57, suggesting that these solid solutions are all ductile. Among them, the Ni−25%Cu solid solution

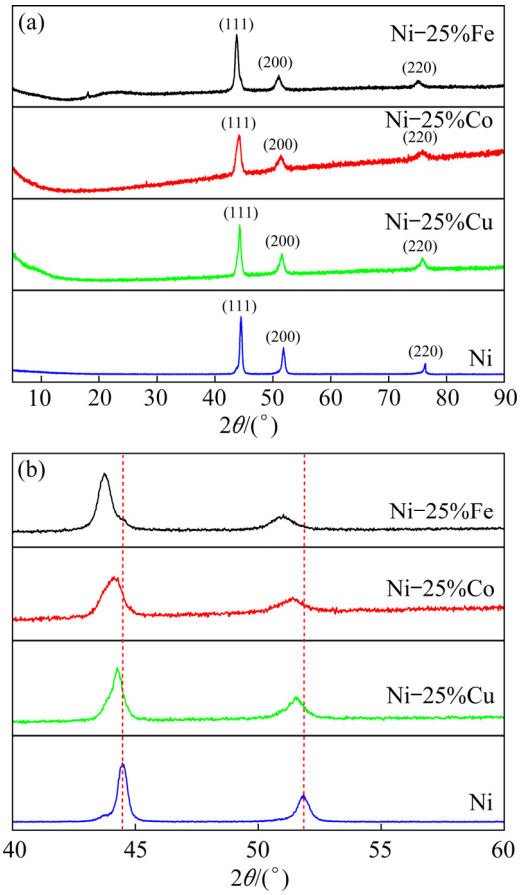

Fig. 1 XRD patterns of as-milled Ni−25%X solid solutions

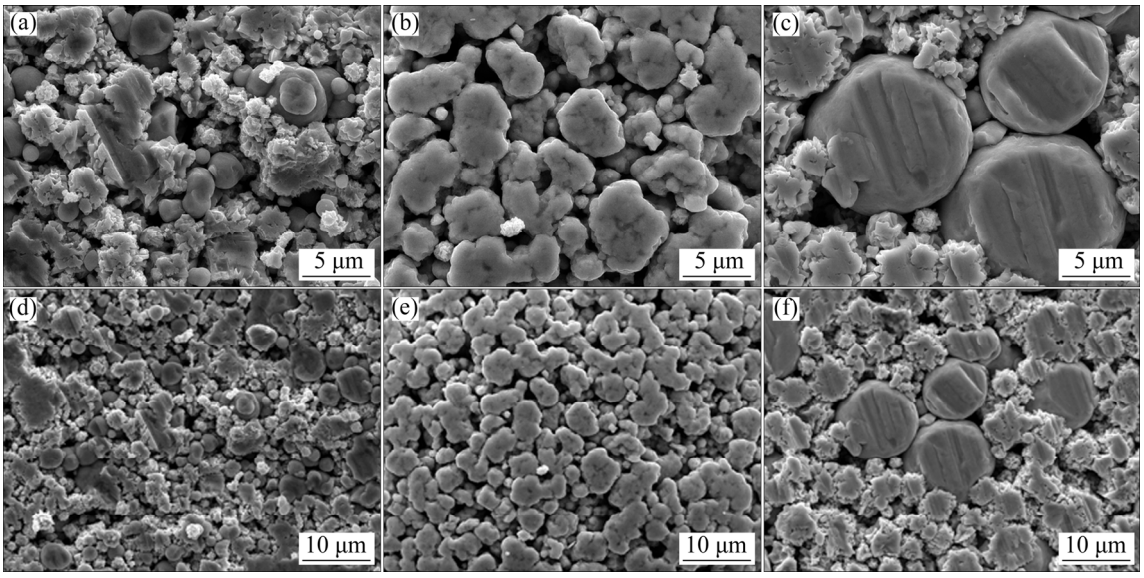

Fig. 2 SEM images of as-milled Ni−25%Fe (a, d), Ni−25%Co (b, e) and Ni−25%Cu (c, f) solid solutions

has the best ductility due to the smallest G/B value, which should be the intrinsic reason for the difficulty to refine Ni−25%Cu particles through ball milling, as shown in Figs. 2(c) and (f).

Figure 3 shows the XRD patterns of as-milled MgH_2/Ni−25%Fe, MgH_2/Ni−25%Co, MgH_2/Ni−25%Cu and pristine MgH_2 composites. All samples contain a major phase of α-MgH_2 and a small amount of γ-MgH_2 phase. Besides, the Ni(X) (X= Fe, Co, Cu) solid solution phases are detected in as-milled MgH_2/Ni−25%X composites, and no other new phases are generated.

Figure 4 presents the SEM images of as-milled MgH_2/Ni−25%X composites with different magnifications. The particle distribution of MgH_2/Ni−25%Fe composite is uneven, and the size is 1−5 μm, as shown in Figs. 4(a) and (d). Comparatively, the particle distribution of MgH_2/Ni−25%Co composite is relatively even, and the size is mainly concentrated in 2−4 μm, as shown in Figs. 4(b) and (e). For MgH_2/Ni−25%Cu composite, the particle distribution is more uniform, and the size is mainly concentrated in 1−3 μm, as shown in Figs. 4(c) and (f).

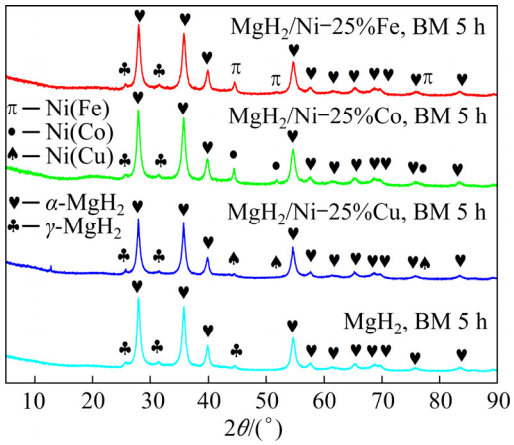

Fig. 3 XRD patterns of as-milled pristine MgH_2 and MgH_2/Ni−25%X composites

3.2 Hydrogen storage properties of MgH_2/Ni−25%X composites

In order to investigate the catalytic effects of different Ni-based solid solutions on the hydrogen storage properties of MgH_2, the dehydrogenation temperatures of the as-milled pristine MgH_2 and MgH_2/Ni−25%X composites are firstly examined by using TPD test. These samples are heated from 20 to 500 °C at a heating rate of 3 °C/min, as shown in Fig. 5. It can be seen that the initial dehydrogenation temperature of as-milled pristine MgH_2 is about 302.7 °C. After Fe, Co and Cu solid-solution, the initial dehydrogenation temperature of MgH_2 is significantly reduced by about 90 °C. When the temperature rises to 305 °C, the dehydrogenation capacity of as-milled pristine MgH_2, MgH_2/Ni−25%Fe, MgH_2/Ni−25%Co and MgH_2/Ni−25%Cu are 0.24, 5.17, 5.87 and 5.81 wt.%, respectively. This means that the Ni-based solid solutions have excellent catalytic effects on the dehydrogenation of MgH_2.

The isothermal hydrogen absorption and desorption kinetics of as-milled pristine MgH_2 and

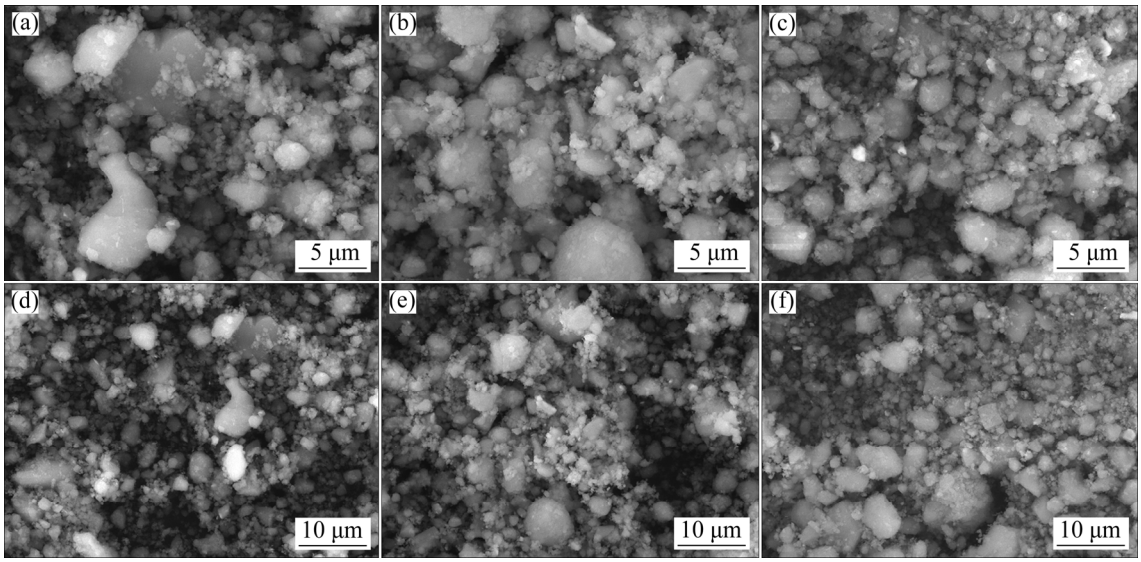

Fig. 4 SEM images of as-milled MgH_2/Ni−25%Fe (a, d), MgH_2/Ni−25%Co (b, e), and MgH_2/Ni−25%Cu (c, f) composites

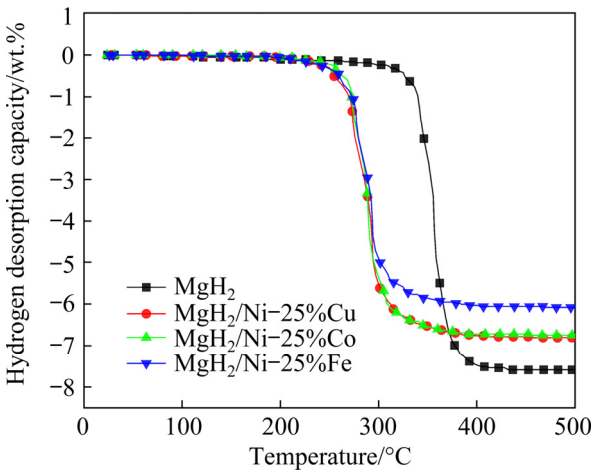

Fig. 5 TPD curves of as-milled pristine MgH_2 and MgH_2/Ni−25%X composites with heating rate of 3 °C/min

MgH_2/Ni−25%X composites are further tested. Figures 6(a)−(f) present the isothermal hydrogenation and dehydrogenation curves of these samples at different temperatures (300, 275, and 250 °C, respectively). At 300 °C, all samples exhibit the excellent hydrogenation kinetic properties, as shown in Fig. 6(a). Among them, the MgH_2/Ni−25%Co composite has the fastest hydrogenation rate, which can absorb 5.50 wt.% hydrogen within 3 min, while the as-milled pristine MgH_2, MgH_2/Ni−25%Cu and MgH_2/Ni−25%Fe composites can only absorb 5.42, 4.47 and 3.46 wt.% hydrogen, respectively. With decreasing temperature, the MgH_2/Ni−25%Co composite still keeps the fastest hydrogenation kinetics. At 275 °C, the MgH_2/Ni−25%Co composite can absorb 5.39 wt.% hydrogen within 3 min, as shown in Fig. 6(c). Even at 250 °C, the MgH_2/Ni−25%Co composite can still absorb 4.27 wt.% hydrogen within 3 min, while the as-milled pristine MgH_2, MgH_2/Ni−25%Cu and MgH_2/Ni−25%Fe composites can only absorb 0.32, 3.73, and 2.97 wt.% hydrogen, respectively. Similar to the hydrogenation case, the MgH_2/Ni−25%Co composite also shows excellent dehydrogenation kinetics. As shown in Fig. 6(b), the MgH_2/Ni−25%Co composite can release 5.19 wt.% hydrogen within 10 min at 300 °C, while as-milled pristine MgH_2, MgH_2/Ni−25%Cu, and MgH_2/Ni−25%Fe composites under the same conditions can only release 1.78, 4.42 and 3.59 wt.% hydrogen, respectively. At 275 °C, the MgH_2/Ni−25%Co composite still maintains excellent dehydrogenation kinetics. It can release 3.84 wt.% hydrogen within 30 min, while as-milled pristine MgH_2 under the same conditions can hardly release hydrogen, as shown in Fig. 6(d). Meanwhile, the MgH_2/Ni−25%Cu and MgH_2/Ni−25%Fe composites can only release 3.44 and 2.99 wt.% hydrogen, respectively. Thus, it can be deduced that the additions of Ni−25%X (X = Fe, Co, Cu) solid solutions improve significantly the hydrogen sorption kinetics properties of MgH_2, and the Ni−25%Co solid solution exhibits the most remarkable catalytic effect.

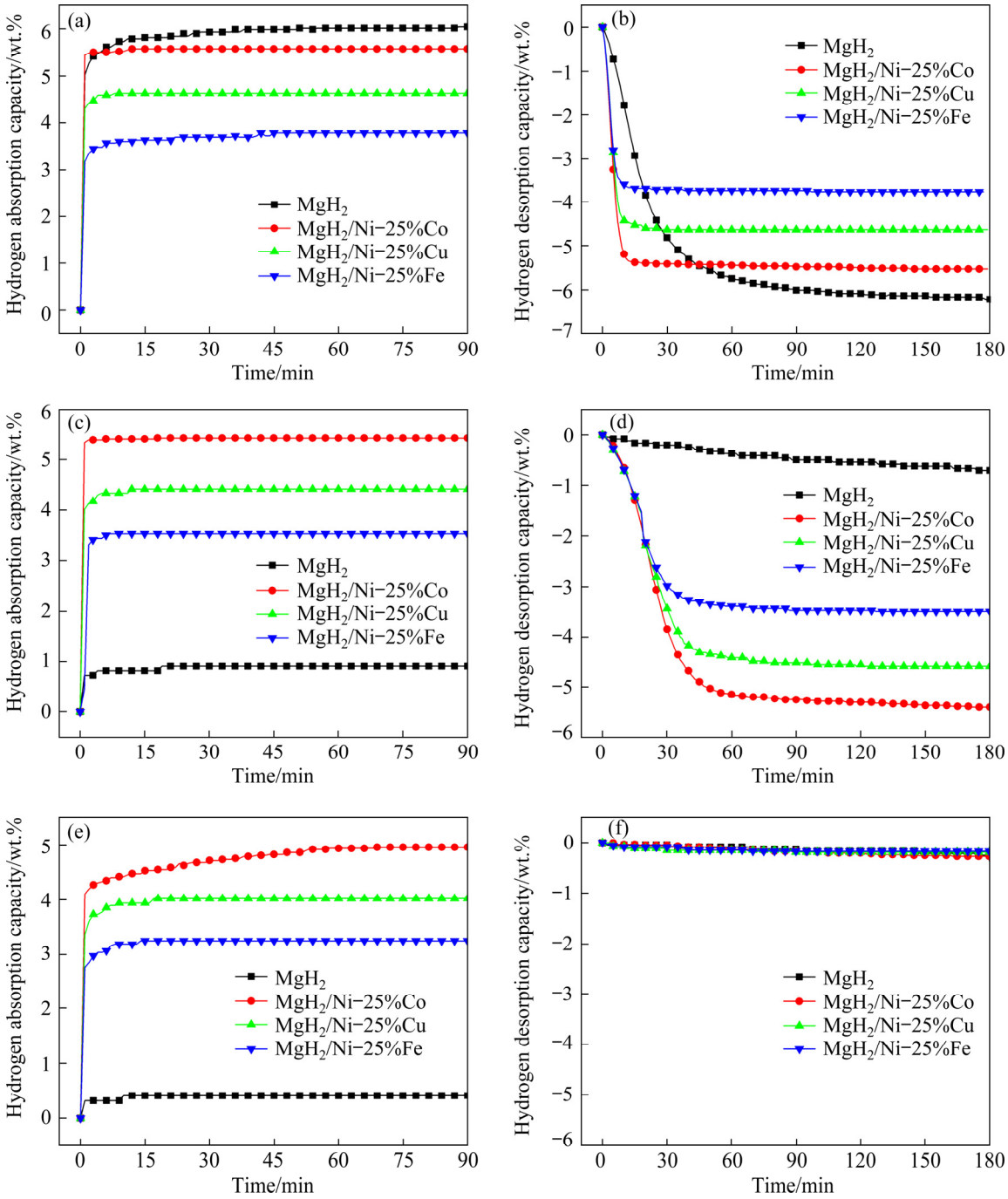

Fig. 6 Hydrogen absorption (a, c, e) and desorption (b, d, f) kinetics curves of as-milled pristine MgH_2 and MgH_2/Ni−25%X composites at 300 °C (a, b), 275 °C (c, d), and 250 °C (e, f), respectively

3.3 Hydrogen storage mechanisms of MgH_2/Ni−25%X composites

In order to disclose the catalytic mechanisms of Ni−25%X solid solutions on hydrogen storage properties of MgH_2, the MgH_2/Ni−25%Co composite was chosen and its microscopic morphology was characterized as shown in Fig. 7. Figure 7(a) shows the TEM image of as-milled MgH_2/Ni−25%Co particles with the size of about 300 nm. Figure 7(b) shows the selected area electron diffraction (SAED) image of particles, and the continuous diffraction rings correspond to MgH_2 with the (111), (101), (211), (220) and (310) planes. Meanwhile, the (111) planes of Ni(Co) are also detected. Figure 7(c) presents the high-resolution transmission electron microscopy (HRTEM) of particles. The lattice fringes with interplanar spacing of 2.50 and 2.22 Å correspond to the (101) and (200) crystal plane of MgH_2, respectively. The lattice fringe with interplanar

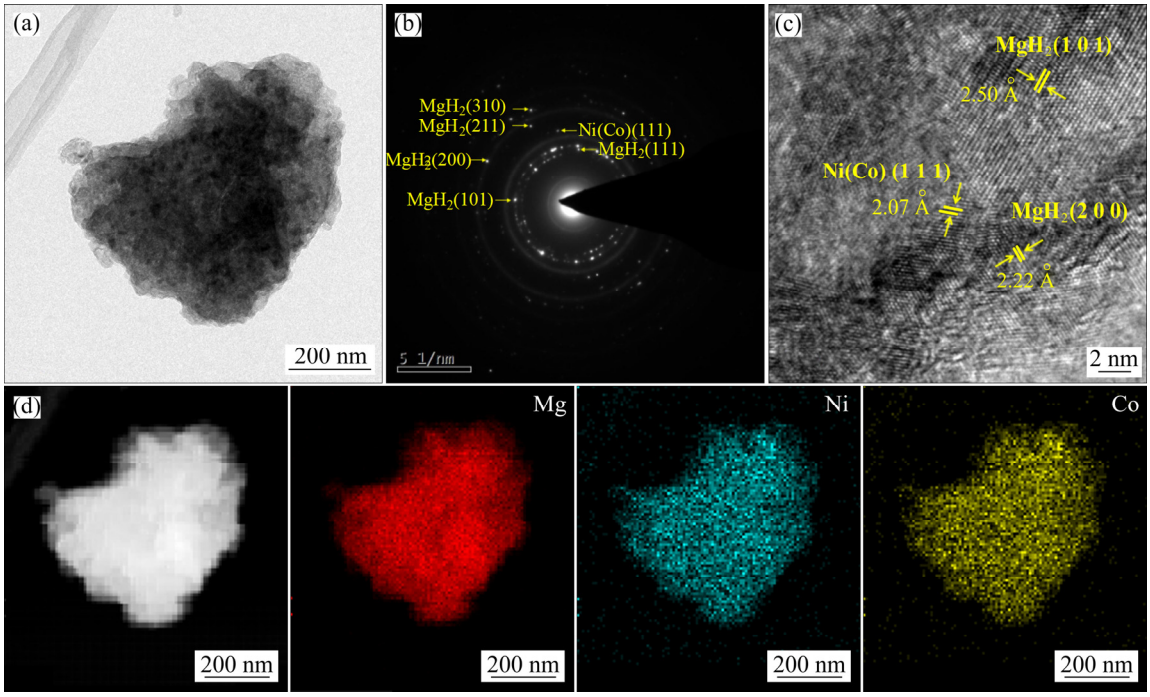

Fig. 7 TEM micrograph (a), selected area electron diffraction pattern (b), high resolution TEM micrograph (c) and corresponding EDS maps (d) of as-milled MgH_2/Ni−25%Co composite

spacing of 2.07 Å is indexed to the (111) crystal plane of Ni(Co) solid solution. The results of SAED and HRTEM verify the presence of MgH_2 and Ni(Co) solid solution in the as-milled sample and no new substances generate during ball milling, which is consistent with Fig. 3. The STEM and the corresponding energy dispersive X-ray spectroscopy (EDS) elemental mapping are further used to characterize the distribution of MgH_2 and Ni(Co) solid solution in the as-milled sample, as shown in Fig. 7(d). It can be seen that Ni(Co) solid solution is homogeneously distributed on MgH_2 matrix.

Figure 8 shows the XRD patterns of as-milled MgH_2/Ni−25%Co composite after dehydrogenation and rehydrogenation. For the dehydrogenated MgH_2/Ni−25%Co composite, Mg is the main phase. Meanwhile, Mg_2Ni(Co) phase is also detected, which indicates that Mg_2Ni(Co) is in-situ formed by the reaction of MgH_2 with Ni−25%Co solid solution during dehydrogenation. After rehydrogenation, the composite contains not only the main phase of MgH_2 but also minor phase of Mg. A small amount of Mg phase is detected probably due to its incomplete hydrogenation. Notably, the Mg_2Ni(Co) phase still appears in the rehydrogenated sample and no other new phase is detected, which means

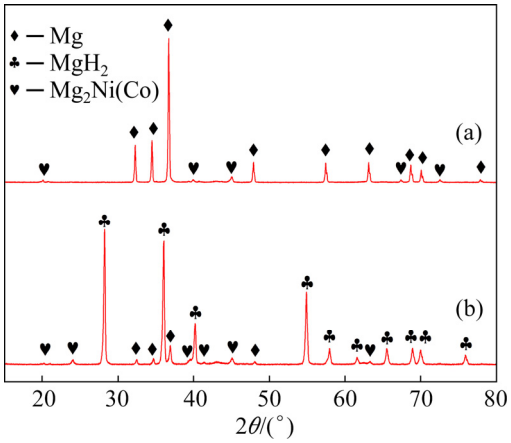

Fig. 8 XRD patterns of as-milled MgH_2/Ni−25%Co composite after dehydrogenation (a) and rehydrogenation (b)

that the in-situ formed Mg_2Ni(Co) is not decomposed during the hydrogenation. The XRD results demonstrate that the in-situ formed Mg_2Ni(Co) phase plays a practical catalytic role in improving the hydrogen absorption and desorption properties of MgH_2/Ni− 25%Co composite. During dehydrogenation/ hydrogenation, the Ni−25%Co solid solution uniformly distributed on the MgH_2 matrix in-situ forms Mg_2Ni(Co), which provides a large number of active nucleation sites and hydrogen diffusion channels for the Mg/MgH_2

system to absorb and release hydrogen. Apparently, the in-situ formed Mg_2Ni(Co) exhibits the typical hydrogen spillover effect on MgH_2 [45].

It is well known that the actual hydrogen absorption/desorption process of Mg/MgH_2 will be affected by the hydrogen absorption/desorption kinetics. In other words, the hydrogen absorption energy barrier needs to be crossed when H_2 molecule breaks from H—H bond to form Mg—H bond with Mg atom. Similarly, the hydrogen desorption energy barrier also needs to be crossed when H atom breaks from Mg—H bond to form H_2 molecule. In order to further interpret the intrinsic reason of different catalytic effects of Ni−25%X solid solutions on hydrogen storage properties of Mg/MgH_2 system, the transition state (TS) of H_2 dissociation/recombination on Mg/MgH_2 surfaces doped with different transition metals X (X=Fe, Co, Ni, Cu) are calculated. Figure 9 shows the optimized initial state (IS) and final state (FS) models of H_2 recombination on pristine MgH_2(110) and the transition metal X-doped MgH_2(110) surfaces. Similarly, Fig. 10 shows the optimized IS and FS models of H_2 dissociation on pristine Mg(0001) and X-doped Mg(0001) surfaces. The calculated energy barrier values are plotted in Fig. 11. For the pristine MgH_2(110), the H_2 recombination energy barrier value is 6.34 eV, as shown in Fig. 11(a). After X doping, the energy barrier values of H_2 recombination on MgH_2(110) surface are decreased significantly, which indicates that the Mg—H bond strength is greatly weakened due to the doping of transition metals. This is consistent with the experimental results from TPD (see Fig. 5) and isothermal dehydrogenation (see Fig. 6). For pristine Mg(0001), the H_2 dissociation energy barrier value is 1.49 eV, as shown in Fig. 11(b). After X doping, the energy barrier values of H_2 dissociation on Mg(0001) surface are also decreased with different degrees. This reveals that the doping of transition metals enhances the catalytic activity of Mg(0001) surface for H_2 dissociation, which is consistent with the experimental results of isothermal hydrogenation (see Fig. 6).

Figure 12 further gives the total densities of states (DOS) of pristine MgH_2(110)/Mg(0001) and the transition metal X (X=Fe, Co, Ni, Cu) doped MgH_2(110)/Mg(0001). In the density of states (DOS) plots, the Fermi level (E_F) is set as zero and used as a reference. From Fig. 12(a), the total DOS of pristine MgH_2(110) surface is mainly distributed

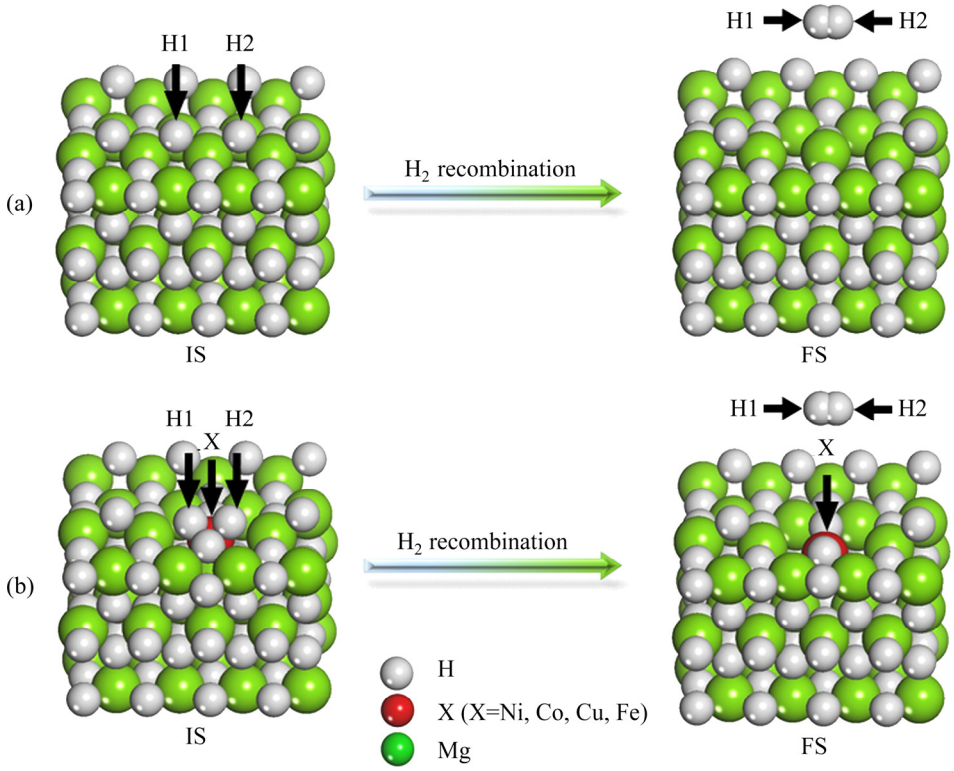

Fig. 9 Optimized initial state (IS) and final state (FS) models of H_2 recombination on pristine MgH_2(110) (a), and transition metal X-doped MgH_2(110) surfaces (b)

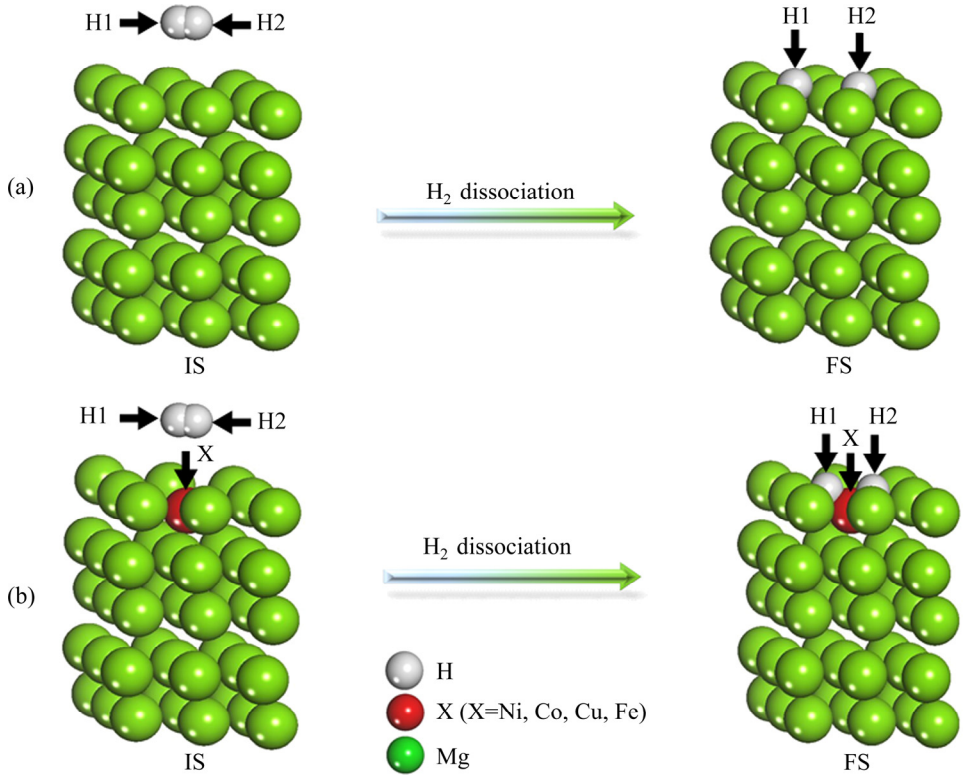

Fig. 10 Optimized initial state (IS) and final state (FS) models of H_2 dissociation on pristine Mg(0001) (a), and transition metal X-doped Mg(0001) surfaces (b)

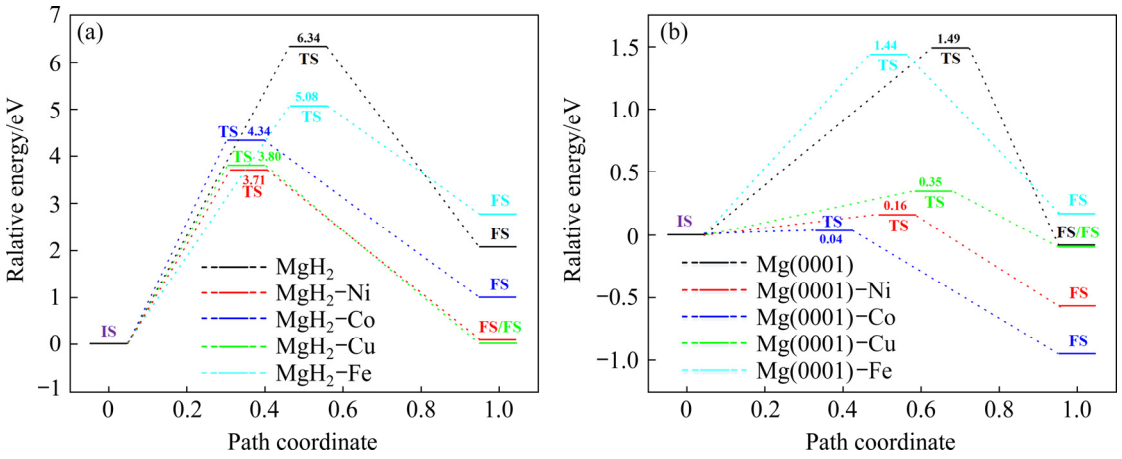

Fig. 11 H_2 recombination (a) and dissociation (b) energy barriers on pristine MgH_2(110)/Mg(0001) and transition metal (Fe, Co, Ni, Cu) doped MgH_2(110)/ Mg(0001) surfaces

in the range of −7.5 to 4.5 eV. As for X-doped MgH_2(110) surfaces, the total DOS moves to the lower energy level, which is mainly distributed in the range of −9.5 to 3.5 eV. More importantly, the energy gap of X-doped MgH_2(110) surfaces near the Fermi level (E_F) is narrower than that of the pristine MgH_2(110) surface. Commonly, the energy gap near the Fermi level (E_F) can be used to judge the structural stability of crystal or surface, the smaller the energy gap near the Fermi level (E_F) means the lower structural stability of crystal or surface [44]. Therefore, the enhanced dehydrogenation ability of MgH_2(110) surface doped with transition metals should be ascribed the weakened structural stability of MgH_2(110) surface after transition metals doping, which leads to the easier hydrogen releasing from MgH_2. Figure 12(b) further compares the total DOS of the first layer atoms of pristine Mg(0001) and X-doped Mg(0001) surfaces. It can be found that the X-doped

Mg(0001) surfaces have higher surface states relative to pristine Mg(0001) surface near the Fermi level (E_F) due to the contribution of 3d orbitals of Fe, Co, Ni and Cu atoms, which indicates that the X-doped Mg(0001) surfaces have a stronger catalytic activity for H_2 dissociation.

Figure 13 further presents the valence charge densities plots of pristine and X-doped MgH_2(110)/Mg(0001) surfaces. Compared with the pristine MgH_2(110) surface, as shown in Fig. 13(a), more electrons cloud overlapping between the transition metal atoms (Fe, Co, Ni, Cu) and the two adjacent H atoms on the surface in X-doped MgH_2(110) surfaces, which means that the bond strength between X and H is stronger than that between Mg and H. The strong bonding interactions between transition metal atoms (Fe, Co, Ni, Cu) and H atoms will result in the weakened bonding strength between H and adjacent Mg atoms, which will be conducive to promoting the release of H atoms and H_2 recombination from MgH_2 surface. From Fig. 13(b), the electron cloud on pristine Mg(0001) surface is relatively flat. Comparatively, the electron on X-doped Mg(0001) surfaces becomes rugged a little. Especially, the slight sinking of electron on the top of transition metals

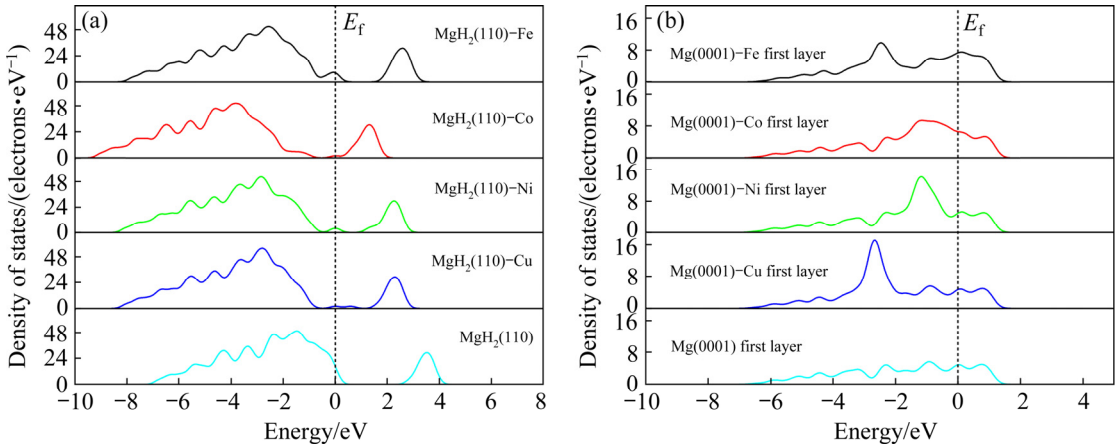

Fig. 12 Total densities of states of pristine and transition metal (Fe, Co, Ni, Cu) doped MgH_2(110) surfaces (a), and total densities of states of the first layer of pristine and transition metal (Fe, Co, Ni, Cu) doped Mg(0001) surfaces (b)

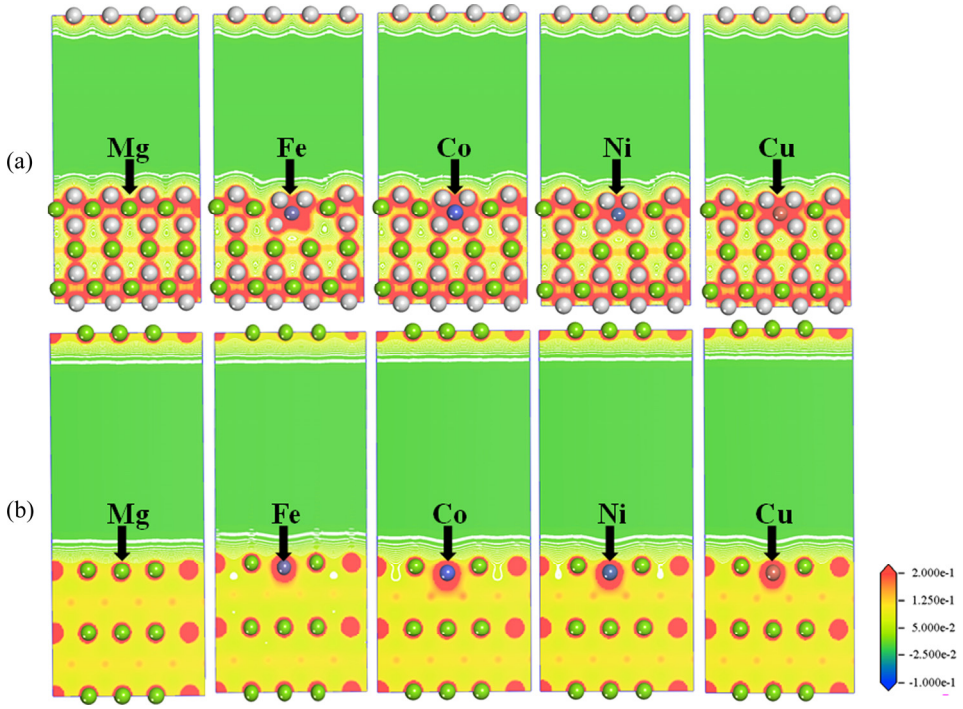

Fig. 13 Valence charge densities of pristine and transition metal (Fe, Co, Ni, Cu) doped MgH_2(110) surfaces (a) and doped Mg(0001) surfaces (b)

can be seen, which may be the underlying reason for enhanced catalytic activity for H_2 dissociation on Mg(0001) surface doped with transition metals.

4 Conclusions

(1) The prepared Ni−25%X (X=Fe, Co, Cu) solid solutions and MgH_2 do not react to form new phases.

(2) As compared with as-milled pristine MgH_2, the initial dehydrogenation temperature of MgH_2/Ni−25%X (X = Fe, Co, Cu) is decreased by about 90 °C. The Ni−25%Co solid solution exhibits the best catalytic effect on the dehydrogenation kinetic properties of MgH_2.

(3) The superior hydrogen sorption kinetics of MgH_2/Ni−25%Co should be ascribed to the actual catalytic role of in-situ formed Mg_2Ni(Co) compounds during hydrogen absorption/desorption. The homogeneous distributed Mg_2Ni(Co) phases significantly promote the dissociation of hydrogen molecules and recombination of hydrogen atoms from Mg/MgH_2.

(4) The first-principles calculations demonstrate that the energy barriers of H_2 dissociation and recombination on Mg(0001)/ MgH_2(110) surfaces are significantly decreased after doping transition metal atoms (Fe, Co, Ni, Cu). The narrowed energy gap of MgH_2(110) surface and enhanced surface state of Mg(0001) surface further interpret the underlying catalytic mechanisms of Ni-based solid solutions.

Acknowledgments

This work was financially supported by the National Natural Science Foundation of China (Nos. 51874049, 51904036), the Science Research Project of Hunan Province Office of Education, China (No. 20A024), the Changsha Science and Technology Program Project (No. kq1907092), the Hunan Provincial Key Laboratory of Materials Protection for Electric Power and Transportation, China (No. 2019CL03), and the Research and Innovation Project of Graduate Students in Changsha University of Science and Technology, China (No. CX2020SS35).

References

[1] MARTINS F, FELGUEIRAS C, SMITKOVÁ M. Fossil fuel energy consumption in European countries [J]. Energy Procedia, 2018, 153: 107−111.

[2] ALVAREZ G E, MARCOVECCHIO M G, AGUIRRE P A. Optimization of the integration among traditional fossil fuels, clean energies, renewable sources, and energy storages: An MILP model for the coupled electric power, hydraulic, and natural gas systems [J]. Computers & Industrial Engineering, 2020, 139: 106141.

[3] LI Li, LIN Jian, WU Nian-yuan, XIE Shan, MENG Chao, ZHENG Ya-nan, WANG Xiao-nan, ZHAO Ying-ru. Review and outlook on the international renewable energy development [J]. Energy and Built Environment, 2020, 3(2): 139−157.

[4] JAIN I P. Hydrogen the fuel for 21st century [J]. International Journal of Hydrogen Energy, 2009, 34(17): 7368−7378.

[5] ZHIZNIN S Z, TIMOKHOV V M, GUSEV A L. Economic aspects of nuclear and hydrogen energy in the world and Russia [J]. International Journal of Hydrogen Energy, 2020, 45(56): 31353−31366.

[6] MAUGERI L. Oil: never cry wolf: why the petroleum age is far from over [J]. Science, 2004, 304(5674): 1114−1115.

[7] ZHANG Jian, YAN Shuai, XIA Guang-lin, ZHOU Xiao-jie, LU Xian-zheng, YU Lin-ping, YU Xue-bin, PENG Ping. Stabilization of low-valence transition metal towards advanced catalytic effects on the hydrogen storage performance of magnesium hydride [J]. Journal of Magnesium and Alloys, 2021, 9(2): 647−657.

[8] YU Chi, FAN Shuan-shi, LANG Xue-mei, WANG Yan-hong, LI Gang, WANG Sheng-long. Hydrogen and chemical energy storage in gas hydrate at mild conditions [J]. International Journal of Hydrogen Energy, 2020, 45(29): 14915−14921.

[9] HAMMAD A, DINCER I. Analysis and assessment of an advanced hydrogen liquefaction system [J]. International Journal of Hydrogen Energy, 2018, 43(2): 1139−1151.

[10] LIU Hai-zhen, XU Li, HAN Yu, CHEN Xin, SHENG Peng, WANG Shu-mao, HUANG Xian-tun, WANG Xin-hua, LU Cheng-lin, LUO Hui, HE Shi-xuan, LAN Zhi-qiang, GUO Jin. Development of a gaseous and solid-state hybrid system for stationary hydrogen energy storage [J]. Green Energy and Environment, 2021, DOI: 10.1016/j.gee.2020.06.006.

[11] JEON S K, KWON O H, JANG H S, RYU K S, NAHM S H, Effect of high pressure hydrogen on the mechanical characteristics of single carbon fiber [J]. Applied Surface Science, 2018, 432: 176−182.

[12] SINGH R, ALTAEE A, GAUTAM S. Nanomaterials in the advancement of hydrogen energy storage [J]. Heliyon, 2020, 6(7): e04487.

[13] ZHANG Jian, QU Hui, YAN Shuai, YU Lin-ping, ZHOU Dian-wu. Dehydrogenation properties and mechanisms of MgH_2−$NiCl_2$ and MgH_2−$NiCl_2$−graphene hydrogen storage composites [J]. Metals and Materials International, 2017, 23(4): 831−837.

[14] KHATABI M E, BHIHI M, LAKHAL M, ABDELLAOUI M, BENYOUSSEF A, KENZ A E, LOULIDI M. Enhanced hydrogen sorption kinetics of co-doped MgH_2 hydrides [J]. Computational Materials Science, 2018, 152: 192−195.

[15] ZHANG Jian, QU Hui, WU Gang, SONG Liu-bin, YU

Xiao-feng, ZHOU Dian-wu. Remarkably enhanced dehydrogenation properties and mechanisms of MgH_2 by sequential-doping of nickel and graphene [J]. International Journal of Hydrogen Energy, 2016, 41(39): 17433−17441.

[16] ZHANG Jian, YAN Shuai, YU Lin-ping, ZHOU Xiao-jie, ZHOU Tao, PENG Ping. Enhanced hydrogen storage properties and mechanisms of magnesium hydride modified by transition metal dissolved magnesium oxides [J]. International Journal of Hydrogen Energy, 2018, 43(48): 21864−21873.

[17] MENG Qiu-fang, HUANG Yu-qin, YE Ji-kai, XIA Guang-lin, WANG Gao-feng, DONG Lin-xi, YANG Zun-xian, YU Xue-bin. Electrospun carbon nanofibers with in-situ encapsulated Ni nanoparticles as catalyst for enhanced hydrogen storage of MgH_2 [J]. Journal of Alloys and Compounds, 2021, 851: 156874.

[18] WANG Peng, WANG Ze-xuan, TIAN Zhi-hui, XIA Chao-qun, YANG Tai, LIANG Chun-yong, LI Qiang. Enhanced hydrogen absorption and desorption properties of MgH_2 with NiS_2: The catalytic effect of in-situ formed MgS and Mg_2NiH_4 phases [J]. Renewable Energy, 2020, 160: 409−417.

[19] ZGANG Huai-wei, BAO Liang, QI Jian-bo, XUAN Wei-dong, FU Li, YUAN Yong-jun. Effects of nano-molybdenum coatings on the hydrogen storage properties of La−Mg−Ni based alloys [J]. Renewable Energy, 2020, 157: 1053−1060.

[20] YAO Peng-yang, JIANG Ying, LIU Yang, WU Cheng-zhang, CHOU Kuo-Chih, LYU Tao, LI Qian. Catalytic effect of Ni@rGO on the hydrogen storage properties of MgH_2 [J]. Journal of Magnesium and Alloys, 2020, 8: 461−471.

[21] DING Xin, CHEN Rui-run, CHEN Xiao-yu, CAO Wen-chao, SU Yan-qing, DING Hong-sheng, GUO Jing-jie. Formation of Mg_2Ni/Cu phase and de-/hydrogenation behavior of $Mg_{91}Ni_{9-x}Cu_x$ alloy at moderate temperatures [J]. Renewable Energy, 2020, 166: 81−90.

[22] HUANG T, HUANG X, HU C, WANG J, LIU H, MA Z, ZOU J, DING W. Enhancing hydrogen storage properties of MgH_2 through addition of Ni/$CoMoO_4$ nanorods [J]. Materials Today Energy, 2021, 19: 100613.

[23] SINGH S, BHATNAGAR A, SHUKLA V, VISHWAKARMA A K, SONI P K, VERMA S K, SHAZ M A, SINHA A S K, SRIVASTAVA O N. Ternary transition metal alloy FeCoNi nanoparticles on graphene as new catalyst for hydrogen sorption in MgH_2 [J]. International Journal of Hydrogen Energy, 2020, 45(1): 774−786.

[24] ZHANG Liu-ting, LU Xiong, SUN Ze, YAN Nian-hua, YU Hai-jie, LU Zhi-yu, ZHU Xin-qiao. Superior catalytic effect of facile synthesized $LaNi_{4.5}Mn_{0.5}$ submicro-particles on the hydrogen storage properties of MgH_2 [J]. Journal of Alloys and Compounds, 2020, 844: 156069.

[25] YONG Hui, WEI Xin, HU Ji-fan, YUAN Ze-ming, WU Ming, ZHAO Dong-liang, ZHANG Yang-huan. Influence of Fe@C composite catalyst on the hydrogen storage properties of Mg−Ce−Y based alloy [J]. Renewable Energy, 2020, 162: 2153−2165.

[26] LIU Jiang-chuan, MA Zhong-liang, LIU Zhi-bing, TANG Qin-ke, ZHU Yun-feng, LIN Huai-jun, ZHANG Yao, ZHANG Ji-guang, LIU Ya-na, LI Li-quan. Synergistic effect of rGO supported Ni_3Fe on hydrogen storage performance of MgH_2 [J]. International Journal of Hydrogen Energy, 2020, 45(33): 16622−16633.

[27] YONG Hui, GUO Shi-hai, YUAN Ze-ming, QI Yan, ZHAO Dong-liang, ZHANG Yang-huan. Catalytic effect of in situ formed Mg_2Ni and REH_x (RE: Ce and Y) on thermodynamics and kinetics of Mg−RE−Ni hydrogen storage alloy [J]. Renewable Energy, 2020, 157: 828−839.

[28] LI Li, JIANG Gao-xue, TIAN Huan-rong, WANG Yi-jing. Effect of the hierarchical Co@C nanoflowers on the hydrogen storage properties of MgH_2 [J]. International Journal of Hydrogen Energy, 2017, 42(47): 28464−28472.

[29] ZHANG Jian, YAN Shuai, QU Hui. Recent progress in magnesium hydride modified through catalysis and nanoconfinement [J]. International Journal of Hydrogen Energy, 2018, 43(3): 1545−1565.

[30] ZHANG Qiu-yu, HUANG Yi-ke, MA Tian-cai, LI Ke, YE Fei, WANG Xue-chao, JIAO Li-fang, YUAN Hua-tang, WANG Yi-jing. Facile synthesis of small MgH_2 nanoparticles confined in different carbon materials for hydrogen storage [J]. Journal of Alloys and Compounds, 2020, 825: 153953.

[31] EL-ESKANDARANY M S, ALMATROUK H S, SHABAN E, AL-DUWEESH A. Effect of the nanocatalysts on the thermal stability and hydrogenation/dehydrogenation kinetics of MgH_2 nanocrystalline powders [J]. Materials Today: Proceedings, 2016, 3: 2608−2616.

[32] LIU Mei-jia, ZHAO Shu-chun, XIAO Xue-zhang, CHEN Man, SUN Cheng-hua, YAO Zhen-dong, HU Zhen-can, CHEN Li-xin. Novel 1D carbon nanotubes uniformly wrapped nanoscale MgH_2 for efficient hydrogen storage cycling performances with extreme high gravimetric and volumetric capacities [J]. Nano Energy, 2019, 61: 540−549.

[33] JIA Yi, YAO Xiang-dong. Carbon scaffold modified by metal (Ni) or non-metal (N) to enhance hydrogen storage of MgH_2 through nanoconfinement [J]. International Journal of Hydrogen Energy, 2017, 42(36): 22933−22941.

[34] EL-ESKANDARANY M S, SHABAN E, AL-MATROUK H, BEHBEHANI M, ALKANDARY A, ALDAKHEEL F, ALI N, AHMED S A. Structure, morphology and hydrogen storage kinetics of nanocomposite MgH_2/10wt.%$ZrNi_5$ powders [J]. Materials Today Energy, 2017, 3: 60−71.

[35] ZHANG Yang-huan, LI Xu-feng, CAI Ying, QI Yan, GUO Shi-hai, ZHAO Dong-liang. Improved hydrogen storage performances of Mg−Y−Ni−Cu alloys by melt spinning [J]. Renewable Energy, 2019, 138: 263−271.

[36] ZHANG Jian, YAO Yuan, HE Liu, ZHOU Xiao-jie, YU Lin-ping, LU Xian-zheng, PENG Ping. Hydrogen storage properties and mechanisms of as-cast, homogenized and ECAP processed $Mg_{98.5}Y_1Zn_{0.5}$ alloys containing LPSO phase [J]. Energy, 2021, 217: 119315.

[37] YANG Tai, LI Qiang, LIU Ning, LIANG Chun-yong, YIN Fu-xing, ZHANG Yang-huan. Improved hydrogen absorption and desorption kinetics of magnesium-based alloy via addition of yttrium [J]. Journal of Power Sources, 2018, 378: 636−645.

[38] ZHANG Yang-huan, WANG Peng-peng, HOU Zhong-hui, YUAN Ze-ming, QI Yan, GUO Shi-hai. Structure and

hydrogen storage characteristics of as-spun Mg−Y−Ni−Cu alloys [J]. Journal of Materials Science & Technology, 2019, 35(8): 1727−1734.

[39] QI Yan, LI Xu-feng, YUAN Ze-ming, CAI Ying, GUO Shi-hai, ZHANG Yang-huan. Structure and hydrogen storage performances of La−Mg−Ni−Cu alloys prepared by melt spinning [J]. International Journal of Hydrogen Energy, 2019, 44(11): 5399−5407.

[40] ZHANG Yang-huan, WANG Peng-peng, ZHANG Wei, BU Weng-gang, QI Yan, Guo Shi-hai. Structure and electrochemical hydrogen storage behaviors of Mg−Ce−Ni−Al-based alloys prepared by mechanical milling [J]. Journal of Rare Earths, 2020, 38(10): 1093−1102.

[41] XIE Li-shuai, LI Jin-shan, ZHANG Tie-bang, KOU Hong-chao. Role of milling time and Ni content on dehydrogenation behavior of MgH_2/Ni composite [J]. Transactions of Nonferrous Metals Society of China, 2017, 27(3): 569−577.

[42] HUANG Tian-ping, HUANG Xu, HU Chuan-zhu, WANG Jie, LIU Hua-bing, XU Hao, SUN Feng-zhan, MA Zhe-wen, ZOU Jian-xin, DING Wen-jiang. MOF-derived Ni nanoparticles dispersed on monolayer MXene as catalyst for improved hydrogen storage kinetics of MgH_2 [J]. Chemical Engineering Journal, 2020, 421: 127851.

[43] CHENG Hong-hui, CHEN Gang, ZHANG Yao, ZHU Yun-feng, LI Li-quan. Boosting low-temperature de/re-hydrogenation performances of MgH_2 with Pd−Ni bimetallic nanoparticles supported by mesoporous carbon [J]. International Journal of Hydrogen Energy, 2019, 44(21): 10777−10787.

[44] ZHAO Ying-yan, ZHU Yun-feng, LIU Jiang-chuan, MA Zhong-liang, ZHANG Ji-guang, LIU Ya-na, LI Yan-hao, LI Li-quan. Enhancing hydrogen storage properties of MgH_2 by core-shell CoNi@C [J]. Journal of Alloys and Compounds, 2021, 862: 158004.

[45] ZHANG Jian, HE Liu, YAO Yuan, ZHOU Xiao-jie, YU Lin-ping, LU Xian-zheng, ZHOU Dian-wu. Catalytic effect and mechanism of NiCu solid solutions on hydrogen storage properties of MgH_2 [J]. Renewable Energy, 2020, 154: 1229−1239.

[46] SEGALL M D, LINDAN P J D, PROBERT M J, PICKARD C J, HASNIP P J, CLARK S J, PAYNE M C. First-principles simulation: ideas, illustrations and the CASTEP code [J]. Journal of Physics: Condensed Matter, 2002, 14(11): 2717−2744.

[47] QIN Chuan-qiong, GU You-song, SUN Xu, WANG Xue-qiang, ZHANG Yue. Structural dependence of piezoelectric size effects and macroscopic polarization in ZnO nanowires: A first-principles study [J]. Nano Research, 2015, 8(6): 2073−2081.

[48] ZHANG Jian, MAO Cong, LONG Chun-guang, CHEN Jian, TANG Kun, ZHANG Ming-jun, PENG Ping. Phase stability, elastic properties and electronic structures of Mg−Y intermetallics from first-principles calculations [J]. Journal of Magnesium and Alloys, 2015, 3(2): 127−133.

[49] WU Meng-meng, WEN Li, TANG Bi-yu, PENG Li-ming, DING Wen-jiang. First-principles study of elastic and electronic properties of $MgZn_2$ and $ScZn_2$ phases in Mg−Sc−Zn alloy [J]. Journal of Alloys and Compounds, 2010, 506(1): 412−417.

基于镍基固溶体催化的氢化镁储氢性能

张 健[1,2]，何 柳[1]，姚 远[1]，周小杰[1]，蒋礼坤[1]，彭 平[3]

1. 长沙理工大学 机械装备高性能智能制造关键技术湖南省重点实验室，长沙 410114；
2. 长沙理工大学 电力与交通材料保护湖南省重点实验室，长沙 410114；
3. 湖南大学 材料与科学工程学院，长沙 410082

摘 要：采用高能球磨制备 Ni−25%X (X=Fe, Co, Cu，摩尔分数)固溶体，然后将其掺杂于 MgH_2 体系中。与球磨纯 MgH_2 相比，MgH_2/Ni−25%X 复合体系初始放氢温度降低近 90 °C，其中，Ni−25%Co 固溶体呈最佳催化效果。球磨 MgH_2/Ni−25%Co 复合体系在 300 °C、10 min 内可释放 5.19%(质量分数)氢，而相同条件下，纯 MgH_2 仅释放 1.78%(质量分数)氢；更为重要的是，放氢后 MgH_2/Ni−25%Co 复合体系在 275 °C、3 min 内可吸收 5.39%(质量分数)氢。MgH_2/Ni−25%Co 体系优异的吸放氢动力学可归因于其在吸/放氢过程中原位形成 Mg_2Ni(Co)化合物的催化作用。第一性原理计算表明，掺杂过渡金属原子后，Mg/MgH_2 体系吸放氢反应能垒显著降低，较好地解释了镍基固溶体催化改善 MgH_2 储氢性能的实验结果。

关键词：MgH_2；镍基固溶体；催化效果；储氢性能；第一性原理计算

(Edited by Xiang-qun LI)